

Collision-induced galaxy formation: semi-analytical model and multi-wavelength predictions

Christophe Balland¹, Julien E. G. Devriendt², and Joseph Silk²

¹Université Paris Sud, IAS-CNRS, Bâtiment 121, 91405 Orsay Cedex, France

²University of Oxford, Astrophysics, Keble Road, Oxford, OX1 3RH, UK

Received ...; accepted ...

ABSTRACT

A semi-analytic model is proposed that couples the Press-Schechter formalism for the number of galaxies with a prescription for galaxy-galaxy interactions that enables to follow the evolution of galaxy morphologies along the Hubble sequence. Within this framework, we calculate the chemo-spectrophotometric evolution of galaxies to obtain spectral energy distributions. We find that such an approach is very successful in reproducing the statistical properties of galaxies as well as their time evolution. We are able to make predictions as a function of galaxy type: for clarity, we restrict ourselves to two categories of galaxies: early and late types that are identified with ellipticals and disks. In our model, irregulars are simply an early stage of galaxy formation. In particular, we obtain good matches for the galaxy counts and redshift distributions of sources from UV to submm wavelengths. We also reproduce the observed cosmic star formation history and the diffuse background radiation, and make predictions as to the epoch and wavelength at which the dust-shrouded star formation of spheroids begins to dominate over the star formation that occurs more quiescently in disks. A new prediction of our model is a rise in the FIR luminosity density with increasing redshift, peaking at about $z \sim 3$, and with a ratio to the local luminosity density $\rho_{L,\nu}(z = z_{peak})/\rho_{L,\nu}(z = 0)$ about 10 times higher than that in the blue (B-band) which peaks near $z \sim 2$.

Key words: cosmology: theory – galaxies:formation – galaxies:interaction

1 INTRODUCTION

In contrast with the local universe, where only 30 % of the bolometric luminosity is released in the IR/submm wavelength range (Soifer & Neugebauer 1991), there is a growing amount of evidence that the high-redshift universe was much more opaque. Indeed, the discovery of the Cosmic Infrared Background (CIRB) at a level ten times higher than the no-evolution predictions based on the IRAS local IR luminosity function, and twice as high as the Cosmic Optical Background obtained from optical counts, has shown that dust extinction and emission are key processes for high-redshift galaxies (Puget et al. 1996; Guiderdoni et al. 1997; Fixsen et al. 1998; Hauser et al. 1998; Schlegel, Finkbeiner & Davis 1998). Deep surveys with the ISO satellite at 15 μm (Oliver et al. 1997; Aussel et al. 1999; Elbaz et al. 1999) and 175 μm (Kawara et al. 1998; Puget et al. 1999), and with the SCUBA instrument at 850 μm (Smail, Ivison & Blain 1997; Barger et al. 1998; Hughes et al. 1998; Eales et al. 1999; Barger, Cowie & Saunders 1999) have begun to resolve the CIRB into its brightest contributors. Although identification and spectroscopic follow-up of submm sources are not easy,

such studies seem to reach the conclusion that an important fraction of these sources are the high-redshift counterparts of the local luminous and ultraluminous IR galaxies (LIRGs and ULIRGs) discovered by IRAS (Smail et al. 1998; Lilly et al. 1999; Barger et al. 1999). In the optical and near-IR window, careful examinations of the Canada–France Redshift Survey (CFRS) galaxies at $z \sim 1$, and Lyman break galaxies at $z \sim 3$ and 4 have revealed a significant amount of extinction (Flores et al. 1999; Steidel et al. 1999; Meurer, Heckman & Calzetti 1999). This has lead to a reassessment of previous estimates of the UV fluxes, and consequently of the star formation rates in these objects, which are now found to be higher by a factor 2 to 5. In light of these observations, one can view the far infrared background as a sink for the hidden aspects of galaxy formation. At optical wavelengths, ellipticals and spheroids are old, even at $z \sim 1$. No evidence is seen for either the luminous formation phase, or the early evolution at these wavelengths. One therefore draws the conclusion that ellipticals and, more generally, most spheroids must have formed in dust-shrouded starbursts.

In this paper, we show how separate tracking of disk and spheroid star formation within a simple but explicit cosmo-

Table 1. Parameters of the cosmological model. h is the Hubble constant at present in units of 100 km/s/Mpc. σ_8 is the rms mass fluctuation in spheres of $8h^{-1}$ Mpc.

Ω_0	λ_0	h	σ_8	Ω_B
0.3	0.7	0.65	0.86	$0.02 h^{-2}$

logical framework enables one to substantiate this view and show that current data is consistent with spheroid formation dominating the submillimetre background. In section 2, we briefly describe how we connect the various pieces of our semi-analytic model together, to differentiate between spheroids and disk galaxies and use the STARDUST model galaxy spectra (Devriendt, Guiderdoni & Sadat 1999) to make the link with observations. The approach is very similar in spirit to that of Devriendt & Guiderdoni (2000) - DG00 hereafter, so we point out the differences/improvements with respect to this previous work. Section 3 presents the results obtained with this new implementation of collision-induced galaxy formation. Finally, we put our work in context with other studies and draw conclusions in Section 4.

2 OVERVIEW OF THE MODEL

2.1 Cosmological framework

To match the combined observations of the cosmic microwave background anisotropies on sub-degree scales by BOOMERanG (de Bernardis et al. 2000) and MAXIMA (Balbi et al. 2000), and of high-redshift supernovae (Riess et al. 1998; Schmidt et al. 1998; Perlmutter et al. 1999), we have chosen a flat universe model with a cosmological constant. More specifically, the ratio of total matter density to critical density and the reduced cosmological constant are taken to be $\Omega_0 = 0.3$ and $\lambda_0 = 0.7$ respectively. The Hubble constant H_0 was chosen to lie within the error bar quoted by the Hubble Space Telescope key project value (Freedman et al. 2001). The value of $\Omega_B = 0.02 h^{-2}$ is the one currently favored by various cosmological probes of Big Bang nucleosynthesis (Bania et al. 2002). Finally the normalization of our non-tilted primordial Harrison-Zeldovich power spectrum $\sigma_8 = 0.86$ ensures fair agreement both with the amplitude of the cosmic background radiation measured by COBE and the local cluster abundance. We note that recent cluster surveys seem to favor slightly lower values around $\sigma_8 \sim 0.73$ (e.g. Lahav et al. 2002) but our conclusions are quite insensitive to a change of 20 % in any of the parameters presented in table 1.

In the semi-analytical *ab initio* approach that we outline in the next section, galaxies form from Gaussian random density fluctuations in the primordial matter distribution, dominated by cold dark matter (CDM). To follow a bound perturbation, we use the well known spherical top-hat collapse model: a homogeneous spherical perturbation grows along with the expanding universe, until self-gravity results in turn around and (non-dissipative) collapse. We then compute the number of perturbations of a given mass which collapse at a given redshift using the standard Press & Schechter (1974) prescription and starting with a primordial power spectrum for the density field given by Bardeen et

al. (1986), corrected for the presence of baryons (Sugiyama 1995). Note that this is slightly different from Devriendt & Guiderdoni (2000), where the prescription to compute the number of collapsed haloes was given by the peaks formalism developed in Bardeen et al. (1986).

2.2 A simple semi-analytic model

To make contact with observations, star formation and spectral evolution must be incorporated. We follow the general framework described by White & Frenk (1991), that is to say, within virialized dark matter halos, we let gas cool radiatively, settle into a disk and form stars. Technical details about the semi-empirical recipes used to model the different astrophysical processes are given in DG00. Chemical and spectral evolution are then computed with the STARDUST model from Devriendt et al. (1999). Detailed references can be looked up in this paper, but, as our results in the far-IR/submm crucially depend upon it, we mention that the dust absorption and emission model implemented in STARDUST is the 3-component model of Désert, Boulanger & Puget (1990), which includes PAHs, very small grains and large grains. Combined with the empirical correlation of the bolometric IR luminosity with IRAS colours, this allows us to self-consistently link the optical and the far-IR/submm windows.

We emphasize that, as discussed in details by DG00, there are three key parameters in such models, the star formation efficiency β^{-1} , the feedback efficiency ϵ_{SN} and the extent of the gaseous disks f_c . We take parameter values that are fairly similar to the ones used by these authors, with $\beta = 60$, $\epsilon_{SN} = 0.2$ and $f_c = 5$. These values are well within the uncertainties of observations by Kennicutt (1998) and Bosma (1981) for the star formation efficiency and the gaseous extent of cold disks, respectively. Numerical simulations by e.g. Thornton et al. (1998) tend to give values closer to 0.1 for feedback efficiency; however our higher value is a consequence of an attempt to reduce the number of small objects overestimated by the Press-Schechter prescription, as well as a means to cure the “cooling catastrophe”, where too much gas cools in low mass halos at high redshift. The qualitative effect of each of these parameters can be summed up in the following way:

- Increasing β decreases the normalisation and faint-end slope of the optical and IR counts, because star formation is reduced and takes place at lower redshift.
- Increasing ϵ_{SN} decreases the normalisation and faint-end slope of the optical and IR counts by quenching star formation in higher and higher mass galaxies that form on average at lower and lower redshifts.
- Increasing f_c means increasing the normalisation of the optical counts, and decreasing that of the IR counts, since this is equivalent to reducing extinction.

The main drawback of DG00 is their modelling of ultraluminous dusty starbursts: they use an *ad hoc* fraction of massive objects F , calibrated locally on the IRAS luminosity function and which is evolving with redshift as $F \propto (1+z)^6$. In this paper, we replace this “recipe” by a physically motivated collision model which allows us to differentiate between disks and ellipticals.

2.3 Modelling galaxy types

To separate disk galaxies from spheroids we use the prescription proposed in Balland, Silk & Schaeffer (1998) - BSS98 hereafter. It is based on the amount of energy exchanged by a galaxy with its neighbours via gravitational interactions during its lifetime. Interactions are modelled as rapid non-merging collisions following the Spitzer impulse approximation (Spitzer 1958). If we denote by $\dot{\Delta}$ the instantaneous relative rate of energy exchange, $(1/E)dE/dt$, at epoch t , the cumulative effect of interactions occurring throughout the galaxy lifetime (from its birth at redshift z_{nl} to the redshift z of observation) is obtained by integration:

$$\Delta \equiv \int \frac{dE}{E} = \int_{z_{nl}}^z \dot{\Delta} \frac{dt}{dz} dz \quad (1)$$

In the above expression, the main parameters describing an interaction (impact parameter, relative velocity between the interacting galaxies, relative mass, number density of neighbouring galaxies) enter through the quantity $\dot{\Delta}$. The scalings with these parameters are derived from the numerical simulations of Aguilar & White (1985). In this way, it is possible to overcome the difficulty of modelling analytically the details of the interaction, which is a highly non-linear process.

The effects of cosmology enter equation (1) via the conversion of the lookback time t into redshift z and the scaling of the interaction parameters with redshift. For instance, in the present cosmology (see table 1), the relative velocity between two interacting galaxies is given by:

$$v = v_0 \sqrt{\Omega_0(1+z) + \lambda_0(1+z)^{-2}}. \quad (2)$$

The evaluation of equation (1) for a galaxy in the field (see BSS98 for details) gives (in a flat, $\Omega_0 + \lambda_0 = 1$, universe):

$$\begin{aligned} \Delta(z) = \Delta_* \Omega_0 & \left\{ \frac{(1+z_{nl})^3 - (1+z)^3}{\Omega_0^2} \right. \\ & - \frac{\lambda_0^2}{\Omega_0^2} \left[\frac{(1+z)^3 - (1+z_{nl})^3}{(\Omega_0(1+z_{nl})^3 + \lambda_0)(\Omega_0(1+z)^3 + \lambda_0)} \right] \\ & \left. - 2 \frac{\lambda_0}{\Omega_0^3} \ln \left[\frac{\Omega_0(1+z_{nl})^3 + \lambda_0}{\Omega_0(1+z)^3 + \lambda_0} \right] \right\} \end{aligned} \quad (3)$$

with $\Delta_* \approx 1.35 \times 10^{-4}$ for $h = 0.65$. It is easy to verify that in the limit $\lambda_0 \rightarrow 0$ equation (3) reduces to $\Delta(z) = \Delta_*[(1+z_{nl})^3 - (1+z)^3]$ which is the result for an $\Omega_0 = 1$ universe (BSS98).

Morphological types are then defined according to the value of Δ using the following rules:

- Galaxies for which Δ is lower than a certain threshold value Δ_{spi} are identified as disks: they correspond to galaxies having experienced few, if any, interactions and consequently have a small Δ .
- Galaxies for which Δ is higher than a certain threshold value $\Delta_{ell} > \Delta_{spi}$ are identified as ellipticals: they correspond to galaxies having undergone substantial energy exchange during their lifetime.
- Galaxies such that $\Delta_{spi} < \Delta(z) < \Delta_{ell}$ are identified as S0 galaxies.

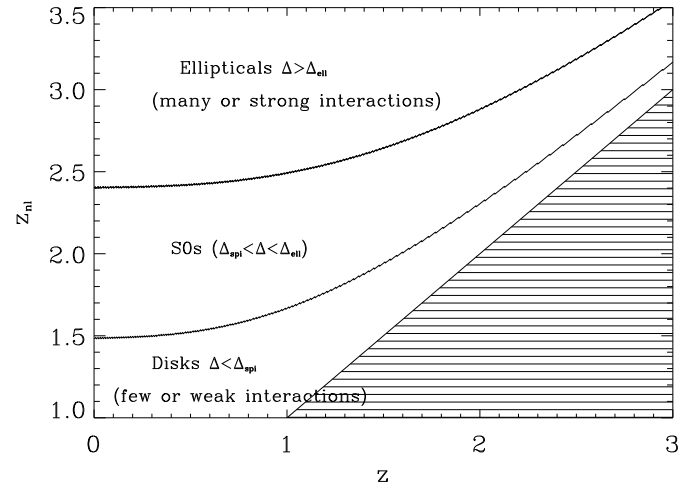


Figure 1. (z_{nl}, z) plane. The upper solid curve is for $\Delta = \Delta_{ell}$ and the lower one for $\Delta = \Delta_{spi}$. The upper region is the locus for galaxies having experienced high energy exchanges due to gravitational interactions since they turned non-linear (the ellipticals region according to the present model), the lower region is the locus for low energy exchange (the disks region). In between, one finds the region for S0s. The hatched area is the region for which $z > z_{nl}$ and is therefore not populated by galaxies.

The values of Δ_{spi} and Δ_{ell} are fixed by requiring that the model produces the observed amount of each type in the field at the present epoch. Typical values are $\Delta_{spi} \approx 3.10^{-3}$ and $\Delta_{ell} \approx 10^{-2}$, and are not very sensitive to the cosmological model assumed (standard or Λ CDM). The above conditions on Δ can then be inverted to obtain conditions on the formation redshift $z_{nl}(z)$ of galaxy types. It is important to realize that the formation redshift of a galaxy of a given type at epoch z depends on z . That is to say that in our model the morphology of a galaxy is not fixed once and for all by initial conditions but, on the contrary, it evolves progressively from late-type to early-type. For instance, the condition for a galaxy to be elliptical at redshift z is that its formation redshift z_{nl} is such that:

$$z_{nl} > z_{ell}(z) \quad (4)$$

where $z_{ell}(z)$ is defined by equating $\Delta(z)$ to Δ_{ell} and solving for z_{nl} . Equivalently, spirals at epoch z are those galaxies that turned non-linear at an epoch such that:

$$z_{nl} < z_{spi}(z) \quad (5)$$

where $z_{spi}(z)$ is defined by equating $\Delta(z)$ to Δ_{spi} . Finally, S0 galaxies are such that:

$$z_{spi}(z) < z_{nl} < z_{ell}(z). \quad (6)$$

Figure 1 illustrates the way morphological types are defined in this model. The formation redshift is shown as a function of the epoch z considered. The solid curves are obtained for $\Delta(z) = \Delta_{ell}$ (upper) and $\Delta(z) = \Delta_{spi}$ (lower). Ellipticals occupy the upper region of the (z_{nl}, z) plane, while disks occupy the lower region. S0s are located in between. The hatched area corresponds to $z_{nl} < z$ and is irrelevant.

Consider the example of a galaxy that became non-linear at, say, $z_{nl} = 3$. Figure 1 shows that up to redshift

$z \sim 2.8$ this galaxy is identified as a disk. Between $z \sim 2.2$ and $z \sim 2.8$, the same galaxy has experienced sufficient energy exchange with its neighbours to be identified as an S0 galaxy, but not quite enough to be an elliptical. By $z \sim 2.2$, it has became an elliptical.

Depending on the previously identified morphological type, we decide which galaxies will undergo an “obscure starburst” phase. More specifically, every galaxy identified as an early type galaxy (ellipticals + S0s) is supposed to go through a LIRG/ULIRG phase, whose intensity and duration are essentially controlled by the amount of gas available for star formation. In practice, this dark phase is modelled by setting our three key parameters to $\beta = 1$, $f_c = 1$ and $\epsilon_{SN} = 0.5$, corresponding to high star formation efficiency, high dust opacity, and high feedback efficiency respectively.

3 RESULTS

3.1 Galaxy counts

Looking at figures 2 and 3, one realises that (except in the near IR bands), late type galaxies dominate over early types (compare the dotted curves with the dashed ones in each panel). This domination extends down to the far-IR, with the late-type galaxies still dominating the 175 micron ISOPHOT counts. At longer wavelengths, however, there is a dramatic change: the early-type galaxies completely swamp the contribution from late types. Indeed, one can see on the bottom right panel of figure 3 that the vast majority ($\approx 90\%$) of the SCUBA sources are classified as early types in our model. The reason for such a change of behaviour lies in the well known negative k-correction, which makes galaxies of the same bolometric luminosity as bright for the observer at redshift 5 as at redshift 0.5. This is only important in the submm (here for SCUBA at 850 microns), because the peak emissivity of dust in the source rest frame is between 60 and 100 microns. Therefore, as our S0s/ellipticals approximately form at $z > 2$, the corresponding maxima of emission must be redshifted to wavelengths greater than 180 and 300 microns respectively.

This result is quite robust in the sense that its qualitative features do not depend on the cosmological parameters. However, quantitatively, there is a marked difference: the domination of late type galaxies is more marked in a SCDM model, where galaxies tend to form later on average (see Silk & Devriendt 2000). This remark also applies to the model of DG00, where the phenomenologically evolving ULIRG fraction was the dominant contributor in the far-IR (175 microns).

Although the general agreement of our predicted counts with the multi-wavelength data seems quite impressive, there are several caveats. At 15 microns, for example, one would say that we match the integral counts fairly well (upper left panel of figure 3). But looking more closely, we cannot reproduce the change of slope seen in the ISOCAM differential counts (fig. 4). There are at least a couple of reasons why this could happen. First, the SEDs of the ISOCAM galaxies are different in the mid-IR from the ones used here as a template, which are based on IRAS observations of the local universe. Differential counts are very sensitive to the exact shape of the PAH features, which are crudely modelled here. One could also imagine that the discrepancy is

partly due to the grain size distribution/chemical composition evolution with redshift, as the redshift distribution of ISOCAM galaxies has a median $z \approx 0.7$. We plan to investigate these issues in more detail but that is beyond the scope of this paper. Finally, because of the way interactions are modelled, each early type galaxy undergoes a starburst after its host halo has just collapsed, and it is not obvious that ISOCAM sources (see figure 3) in which the vast majority are LIRGs (not ULIRGs), are properly described by such a violent process. Dynamical interactions (which are not modeled in detail here), triggering multiple milder starbursts, with time delays between them, might provide a more realistic description of these sources and this is another issue we plan to investigate in the future.

3.2 Redshift distributions

Another constraint on our models comes from the redshift distributions. Their shapes seem to quite nicely match the observations in the I band with a mean redshift of the distribution of ~ 0.6 , (see top left panel of figure 5). In the far-IR (60 microns), the agreement with data gathered in the north ecliptic pole region (NEPR) is also fairly convincing. As predicted in Silk & Devriendt (2000), inclusion of the cosmological constant, Λ , has shifted the near-IR and 60 micron peaks towards higher redshifts and produced a high-redshift tail in the I band, bringing the models into closer agreement with the data. Disks and early-types are found in comparable proportion in the I-band, with a slight domination of disks for $z > 0.3$ and up to $z = 1.5$.

There are at least a couple of reasons for this behaviour. First, in this redshift range, spheroids are already old, their star formation rates are very low and therefore their I-band luminosity comes from an old and dim stellar population. Secondly, spheroids in a massive starburst phase at these redshift experience high dust absorption, which reduces significantly their luminosity even in the I band. Going deeper in I magnitude leads to the selection of higher redshift galaxies and we expect that the starburst population to eventually dominate the distribution around $z \approx 2$.

We draw the reader’s attention to the dramatic change occurring in the redshift distribution of sources when going from ISOPHOT to SCUBA, *i.e.* from the far-IR, to the submm window (bottom panels of figure 5). In the far-IR, the vast majority of sources is predicted to lie at fairly low redshifts, whereas in the submm, there is a characteristic double peaked distribution. The first small peak at low redshift is mainly due to disks, as can be seen on the lower right panel of figure 3 ($\lambda_{eff} = 850 \mu\text{m}$). Indeed, the Euclidian tail of the total counts (figure 3) at fluxes above $\sim 10^{-1} \text{ Jy}$ on this figure is clearly due to the domination of local bright disks (dotted line). In contrast, one notes on the lower-right panel of figure 5 an overwhelming domination of the (fainter) sources located at high redshifts, as is also clear from figure 3. Once again, the main driver for this effect is the negative k-correction boosting observed fluxes in the submm wave-bands. Contrary to Devriendt and Guiderdoni (2000) and Lagache et al. (2002), the second peak in the redshift distribution of 175 microns sources (around $z = 1$, see e.g. Lagache et al. (2002)) is missing from the model discussed here. This could either be a result of the STARDUST SEDs being too warm for LIRGs, or of a too rapid evolu-

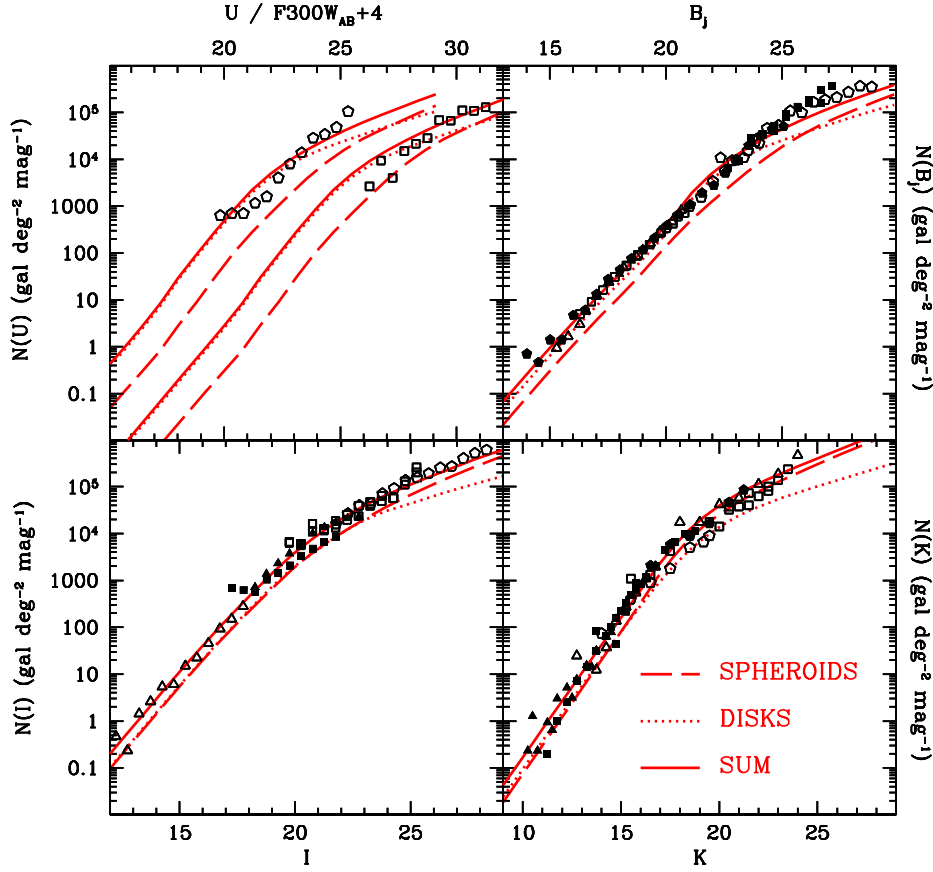


Figure 2. UV/Optical/Near-IR counts from our analytic model, compared to existing data. The dotted curves stand for late type galaxies (disks); the dashed ones for early type galaxies (spheroids); and the solid ones for the sum of both contributions. Data is from Hogg et al. (1997) (U band), Williams et al. (1996) (F300W_{AB}, B & I bands), Arnouts et al. (1997) (B band), Bertin & Dennefeld (1997) (B band), Gardner et al. (1996) (B, I & K bands), Metcalfe et al. (1996) (B band), Weir et al. (1995) (B band), Smail et al. (1995) (I band), Crampton et al. (1995) (I band), Moustakas et al. (1997) (K band), and Djorgovski et al. (1995) (K band).

tion in the number of LIRGs due to our simple modelling of galaxy interactions. Here too, triggering several starbursts per galaxy with delays between them, as happens in realistic galaxy interactions, could alleviate the problem.

3.3 Diffuse background radiation

The background light, as integrated from the multi-wavelength counts, seems to closely match the detection by Puget et al. (1996) and Hauser et al. (1998) in the far-IR/submm window (see figure 6). This tells us that we are not grossly overestimating or underestimating the faint counts, and that the global galaxy luminosity budget from the UV to the submm is likely to be correctly computed. An interesting remark is that this plot clearly shows that one has to go to the submm, around 1500 GHz (about 200 microns), to see the early-type galaxies dominate over the late types. This is a factor 2 shorter in wavelength than found for the SCDM model. At any wavelength shorter than this (except in the near-IR between 2-5 microns), quiescent galaxies, forming up to $\approx 10 M_\odot$ of stars per year dominate the total light emission (as well as the counts). Again that was not

the case with the SCDM model where spirals dominated the whole background below 400 microns.

3.4 Multi-wavelength comoving luminosity densities

Figure 7 shows the comoving luminosity densities predicted by the model from the far-UV (bottom curves) to the far-IR (top curves). It is clear from the figure that there already is a greater amount of evolution in the far-IR than in the UV-optical, and we know from the counts (fig. 3) that the submm must show still more evolution than the far-IR. The agreement with the data is quite satisfactory both at low and high redshift and for all wavelengths. This tells us that the luminosity budget of our galaxies is relatively accurate. Another striking feature is that the model predicts that the spheroid (whether in dusty starburst phase or not) contribution to the comoving luminosity density becomes approximately equal to that of late type galaxies around redshift 2 in the UV and far-IR and as early as $z \sim 1$ in the B-band. As a result, the peak of the comoving luminosity density shows a complex behavior as a function of wavelength, starting

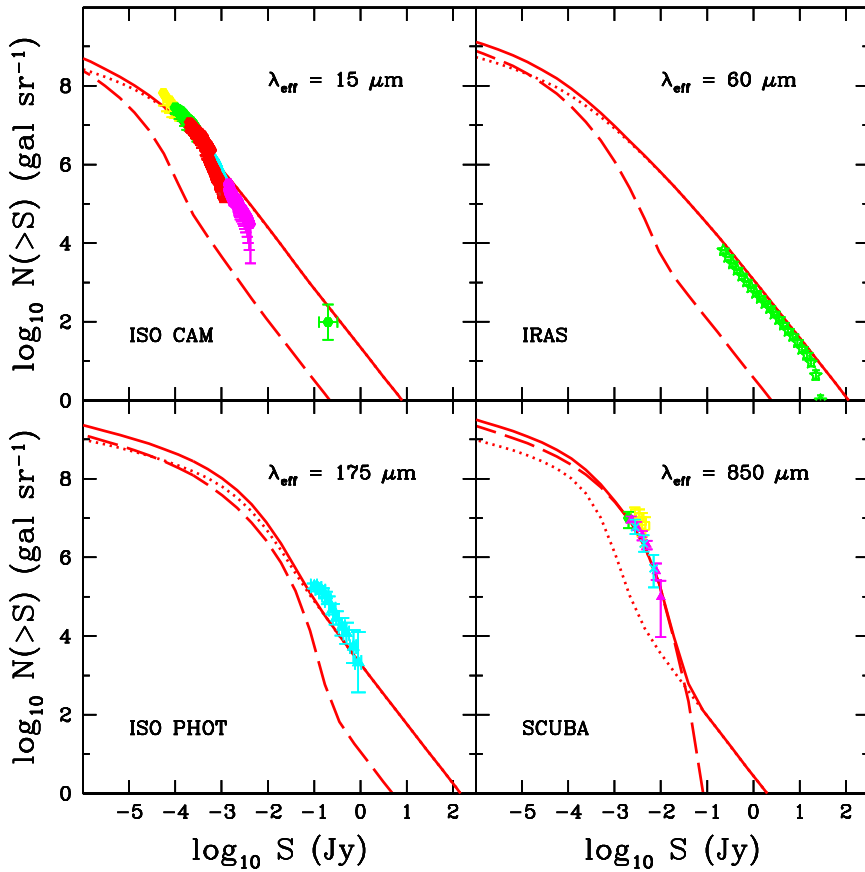


Figure 3. Infrared/submm counts from the analytic model described in the text. Coding for the lines is dotted: late type galaxies (spirals); dashed: early type (ellipticals, S0s); and solid: sum of both contributions. Data are from Elbaz et al. (1999) (15 μm), Kawara et al. (1998), Puget et al. (1999) and Dole et al. (2001) (175 μm), Smail et al. (1997), Eales et al. (1999), Barger et al. (1999), Scott et al. (2002) (850 μm).

around $z \sim 3$ in the UV and falling to $z \sim 2$ in the optical near-IR, before shifting again to higher redshifts ($z \sim 3$) in the far-IR and submm. This reflects the fact that both UV and far-IR luminosities are extremely sensitive to the instantaneous SFR, whereas the optical and near-IR luminosities are tainted by a non-negligible contribution coming from an old stellar population.

3.5 Cosmic star formation history

The predicted comoving star formation rate is compared to observations on figure 8. Empty symbols are observed estimates at various redshifts, uncorrected for dust extinction. Filled symbols indicate dust corrected estimates following the prescription of Somerville, Primack & Faber (2001) based on a luminosity dependant correction likely to be more realistic than the traditional scaling by a constant factor (between 3 to 5) at all z (see their figure 9). The filled point at $z \sim 0.7$ is derived from infrared ISOCAM observations (Flores et al. 1999).

The comoving SFR is in fair agreement with the measured one, and the reasonable amount of K-band light produced (figure 2) makes us confident that we do not over-

produce either stars or metals. However note that at low redshift, the agreement is only for non-dust-corrected data, so the contribution of our spirals (which closely match the non corrected Madau curve at *all* redshifts) might be underestimated in our model. From the perspective of metals only, the star formation rate could be higher, provided that a fair fraction of the heavy elements is ejected into the IGM. The model however predicts a peak in star formation around redshift ~ 3.5 (this is also true for the SCDM case), sensibly higher than what is usually assumed, current data being compatible with a flat star formation rate at redshifts $z > 1$. A more detailed comparison with the SCDM cosmology used in Silk & Devriendt (2000) reveals that the comoving star formation rate increase from $z = 0$ to $z \approx 3$ is steeper in the ΛCDM model, due to the fact that fewer galaxies tend to form on average at low redshifts in such a model. More specifically, this increase in the steepness of the SFR results from:

- a similar high redshift SFR level in a ΛCDM and in a SCDM cosmology because the earlier formation of galaxies in a ΛCDM model is compensated by a higher normalization of the power spectrum in a SCDM model
- a lower contribution to the SFR history at late times in

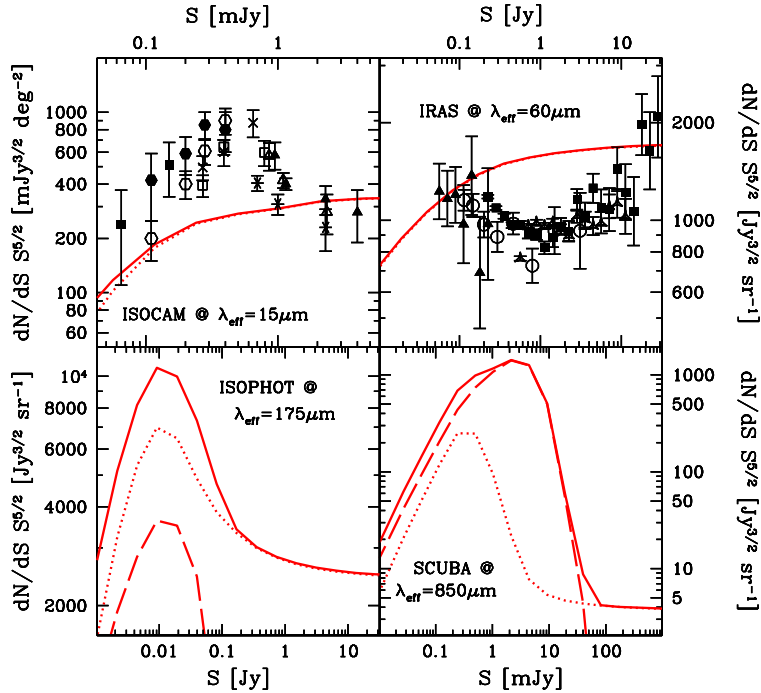


Figure 4. Infrared/submm differential counts from the model. Coding for the lines is dotted: late type galaxies (spirals); dashed: early type (ellipticals, S0s); and solid: sum of both contributions. Data are taken from various ISO surveys described in Elbaz et al. (1999) at 15 μm , and various analysis of IRAS samples (see e.g. Guiderdoni et al. 1998 at 60 μm).

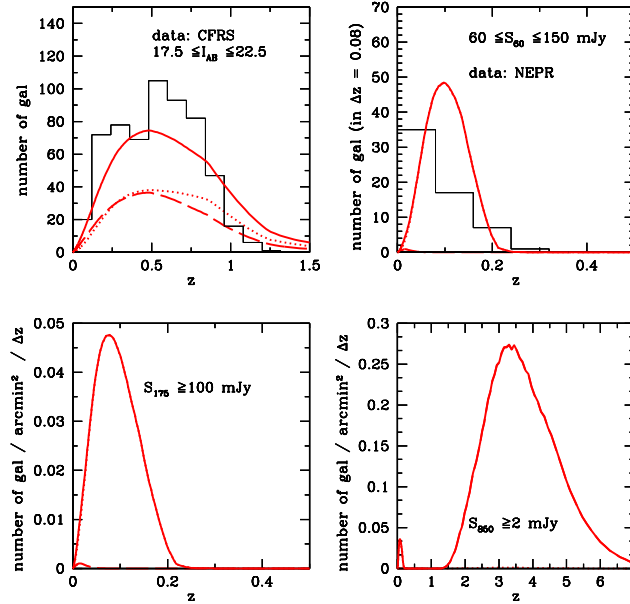


Figure 5. Panchromatic redshift distributions of galaxies predicted by our analytic model. Dotted curves represent late type galaxies (spirals); dashed: early type galaxies (ellipticals, S0s); and solid: the sum of both contributions. Data in the I band (top left panel) is from Crampton et al. (1995) (Canada–France Redshift Survey), whereas at 60 microns, it comes from Ashby et al. (1996) (North Ecliptic Pole Region). In both cases, the model curves have been renormalized to the total number of observed galaxies.

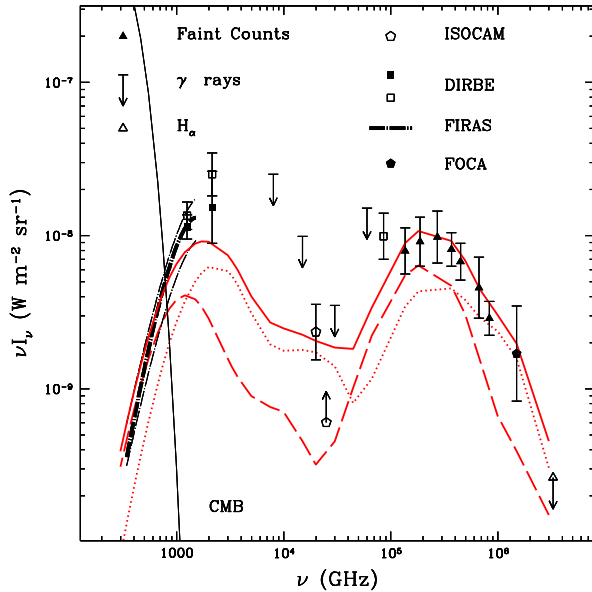


Figure 6. Diffuse background light emitted by star forming galaxies, from the UV to the submm. Coding for the lines is dotted: late type galaxies (disks); dashed: early type galaxies (spheroids); and solid: sum of both contributions. The data sources are indicated on the figure.

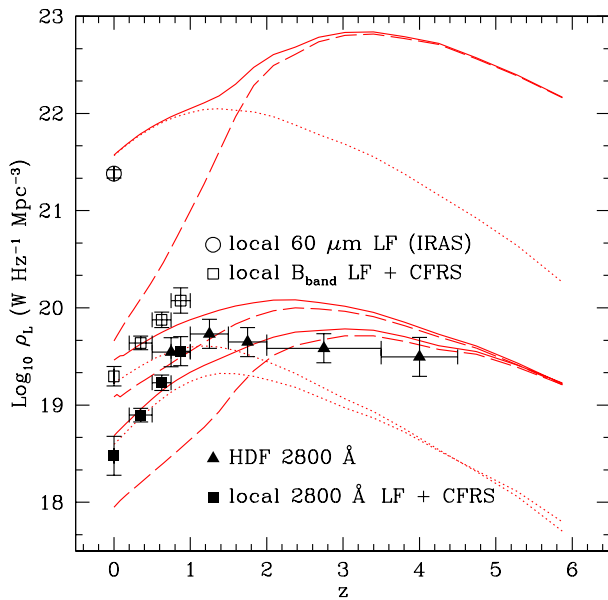


Figure 7. Comoving luminosity densities as a function of redshift. As usual, coding for the lines is dotted: late type galaxies (disks); dashed: early type galaxies (spheroids); and solid: sum of both contributions. The three sets of curves represent predictions of our model at 2800 Å (bottom triplet), 4400 Å (middle triplet) and 60 microns (top triplet). Data sources are indicated on the figure.

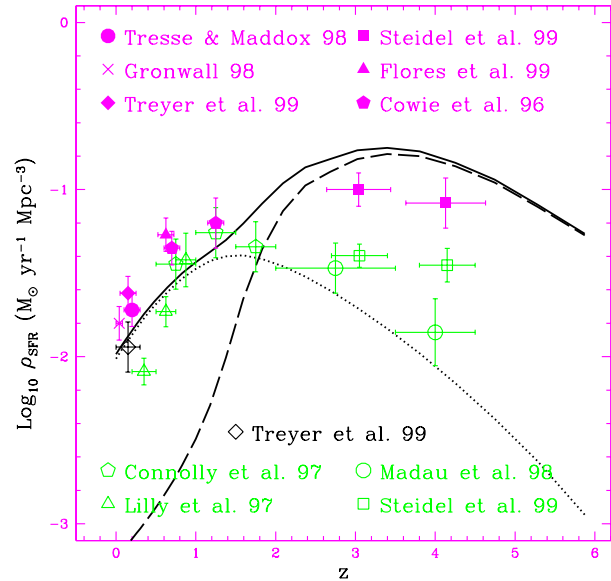


Figure 8. Comoving star formation rate as a function of redshift. The different curves represent the contribution of late type galaxies (spirals: dotted line); early type galaxies (ellipticals, S0s: dashed line); and the sum of both contributions (solid line). Empty symbols give raw measurements of different teams (renormalized to match the cosmological model defined in table 1): circles (Madau, Pozzetti & Dickinson 1998); squares (Steidel et al. 1999); triangles (Lilly et al. 1996) and pentagons (Connolly et al. 1997). Filled diamonds are data from Gronwall (1998); Tresse & Maddox (1998); Treyer et al. (1998); Cowie, Songaila & Barger (1999); Steidel et al. (1999) and are dust-corrected as described in Somerville et al. (2001). The point at $z \sim 0.7$ is derived from far-IR ISOCAM sources (Flores et al. 1999).

the Λ CDM model due to the formation of a smaller number of galaxies than in the SCDM model

This explains why the discrepancy mainly shows up in the spiral population and that, in contrast, the contribution of elliptical galaxies which form much earlier is very similar in both cosmologies (Silk & Devriendt 2000). We argue that the amount of star formation occurring in dust-shrouded objects cannot be much greater than our model predicts in order to avoid overestimating the submm diffuse background (see figure 6). Therefore we emphasize that cosmic star formation has to decrease at redshifts $z \geq 3.5$. Note that this result is strengthened if dust-shrouded AGNs are a major contributor to the submm emission, even though this does not appear to be the case if X-ray characteristics are a reliable AGN monitor (e.g. Barger et al. 2001).

4 CONCLUSIONS

We have implemented the model of BSS98 within the simple semi-analytic model of DG00 in order to describe galaxy collisions on a physical basis. We find that such a combination:

- naturally reproduces galaxy counts at various wavelengths and the diffuse background radiation.

- yields a fair match to existing redshift distributions ranging from the optical (CFRS) to far-IR (IRAS at 60 microns). Furthermore, the model also predicts redshift distributions of sources at still larger wavelengths (ISOPHOT at 175 microns; SCUBA at 850 microns)
- predicts the contribution of morphological types to the previous quantities, with spheroids strongly dominating bright galaxy counts only in the sub-millimetre window (from 450 microns and longwards).
- predicts that the cosmic star formation rate history is dominated by spiral-like objects until redshift 2 where spheroids become the major contributors.

Our results qualitatively agree with the model of the infrared universe presented in Tan, Silk & Balland (1999). We also note good agreement of the main conclusions of the present work with the collisional starburst model of Somerville et al. (2001). This agreement is exemplified in the comparison between our SFR plot (figure 8 of the present paper) and the SFR predicted by their collisional starburst model (their figure 9). It is satisfying that these two approaches give consistent results as it supports the view that galaxy-galaxy collisions in the high redshift universe might have played a dominant role in triggering star formation.

Note however that Somerville et al. fail to account for the submm counts. They find too few highly obscured luminous galaxies. Our model gives satisfactory agreement both in the restframe blue and FIR. This is because we have the freedom, and indeed the motivation from the model, to prolong the duration of the dust-shrouded phase. Because the spheroid collisions are extended over several Hubble times after the first collision, this is an inevitable consequence of our model. The semi-analytic hierarchical model forms spheroids over a Hubble time at redshift of first collapse of the mass in question. This may not be enough if the dust is dispersed by the ensuing starburst. Introduction of an *ad hoc* delay might solve this. Alternatively one might appeal to additional sources of IR luminosity such as the one that might be associated with AGN formation. All indications however suggest that AGNs do not play a major role in accounting for most of the observed submm sources, as evidenced from the CHANDRA deep fields. In our case we have a physical model that works in the right direction and yields a self-consistent panchromatic explanation of the observed universe both locally and at high redshift.

An important consequence of our model is that the FIR counts and luminosity density are expected to continue to rise with redshift to $z \sim 3$. Hence we predict that a future mission with adequate resolution to avoid source confusion, which sadly may not be the case for ASTROF or SIRTF, will provide an important test of the galaxy collision model.

ACKNOWLEDGMENTS

We thank Guilaine Lagache, Hervé Dole and Jean-Loup Puget for providing us with their results before publication. J.D. acknowledges support from the Leverhulme trust.

REFERENCES

Aguilar L. A., White S. D. M., 1985, ApJ, **295**, 374

Arnouts S., de Lapparent V., Mathez G., Mazure A., Mellier Y., Bertin E., Kruszewski A., 1997, A&A Suppl., **124**, 163

Ashby M. L. N., Hacking P. B., Houck J. R., Soifer B. T., Weisstein E. W., 1996, ApJ, **456**, 428

Aussel H., Elbaz D., Cesarsky C. J., Starck J. L., 1999, in The Universe as Seen by ISO. Eds. P. Cox & M. F. Kessler

Balbi A., et al., 2000, ApJ, **545**, L1

Balland C., Silk J., Schaeffer R., 1998, ApJ, **497**, 541 (**BSS98**)

Bania T. M., Rood R. T., Balser D.S., 2002, Nature, **415**, 54

Bardeen J. M., Bond J. R., Kaiser N., Szalay A. S., 1986, ApJ, **304**, 15

Barger A. J., Cowie L. L., Sanders D. B., Fulton E., Taniguchi Y., Sato Y., Kawara K., Okuda H., 1998, Nature, **394**, 248

Barger A. J., Cowie L. L., Sanders D. B., 1999, ApJ, **518**, L5

Barger A. J., Cowie L. L., Mushotzky R. F., Richards E. A., 2001, Astron. J., **121**, 662

Bertin E., Dennefeld M., 1997, A&A, **317**, 43

Bosma A., 1981, Astron. J., **86**, 1825

Connolly A. J., Szalay A. S., Dickinson M., Subbarao M. U., Brunner R. J., 1997, ApJ, **486**, L11

Cowie L. L., Songaila A., Barger A., 1999, Astron. J., **118**, 603

Crampton D., Le Fèvre O., Lilly S. J., Hammer F., 1995, ApJ, **455**, 96

de Bernardis P., et al., 2000, Nature, **404**, 955

Désert F.-X., Boulanger F., Puget J.-L., 1990, A&A, **237**, 215

Devriendt J. E. G., Guiderdoni B., Sadat R., 1999, A&A, **350**, 381

Devriendt J. E. G., Guiderdoni B., 2000, A&A, **363**, 851 (**DG00**)

Djorgovski S., et al., 1995, ApJ, **438**, L13

Dole H., et al., 2001, A&A, **372**, 364

Eales S., Lilly S., Gear W., Dunne L., Bond J. R., Hammer F., Le Fèvre O., Crampton D., 1999, ApJ, **515**, 518

Elbaz D., et al., 1999, A&A, **351**, L37

Fixsen D. J., Dwek E., Mather J. C., Bennett C. L., Shafer R. A., 1998, ApJ, **508**, 123

Flores H., et al., 1999, ApJ, **517**, 148

Freedman W. L., et al., 2001, ApJ, **553**, 47

Gardner J. P., Sharples R. M., Carrasco B. E., Frenk C. S., 1996, MNRAS, **282**, L1

Gronwall C., 1998, in Thuan T., ed, Dwarf Galaxies and Cosmology. Editions Frontières, [astro-ph/9806240](#)

Guiderdoni B., Bouchet F. R., Puget J.-L., Lagache G., Hivon E., 1997, Nature, **390**, 257

Guiderdoni B., Hivon E., Bouchet F. R., Maffei B., 1998, MNRAS, **295**, 877

Hauser M. G., et al., 1998, ApJ, **508**, 25

Hogg D. W., Pahre M. A. McCarthy J. K., Cohen J. G., Blandford R., Smail I., Soifer B. T., 1997, MNRAS, **288**, 404

Hughes D. H., et al., 1998, Nature, **394**, 241

Kawara K., et al., 1998, A&A, **336**, L9

Kennicutt R. C., 1998, ApJ, **498**, 541

Lagache G., Dole H., Puget J.-L., 2002, MNRAS, in press

Lahav O., et al., 2002, MNRAS, **333**, 961

Lilly S. J., Le Fèvre O., Hammer F., Crampton D., 1996, ApJ, **460**, L1

Lilly S. J., Eales S. A., Gear W. K. P., Hammer F., Le Fèvre O., Crampton D., Bond J. R., Dunne L., 1999, ApJ, **518**, 641

Madau P., Pozzetti L., Dickinson M., 1998, ApJ, **498**, 106

Metcalfe N., Shanks T., Fong R., Gardner J., Roche N., 1996, in IAU symp. 171, New Light on Galaxy Evolution, R. Bender & R. L. Davies eds, Kluwer Academic Publishers, 225

Meurer G. R., Heckman T. M., Calzetti D., 1999, ApJ, **521**, 64

Moustakas L. A., Davis M., Graham J. R., Silk J., Peterson B. A., Yoshii Y., 1997, ApJ, **475**, 445

Oliver S., et al., 1997, MNRAS, **289**, 471

Perlmutter S., et al., 1999, ApJ, **517**, 565

Press W. H., Schechter P., 1974, ApJ, **187**, 425

Puget J.-L., Abergel A., Bernard J.-P., Boulanger F., Burton W. B., Desert F.-X., Hartmann D., 1996, *A&A*, **308**, L5

Puget J.-L., et al., 1999, *A&A*, **345**, 29

Riess A. G., et al., 1998, *Astron. J.*, **116**, 1009

Schlegel D., Finkbeiner D., Davis M., 1998, *ApJ*, **500**, 525

Schmidt B. P., et al., 1998, *ApJ*, **507**, 46

Scott S. E., et al., 2002, *MNRAS*, **331**, 817

Silk J., Devriendt J. E. G., 2000, in IAU symp. 204, The Extra-galactic Infrared Background and its Cosmological Implications, Martin Harwit and Michael G. Hauser eds., in press, [astro-ph/0010460](http://arxiv.org/abs/astro-ph/0010460)

Smail I., Hogg D. W., Yan L., Cohen J. G., 1995, *ApJ*, **449**, L105

Smail I., Ivison R. J., Blain A. W., 1997, *ApJ*, **490**, L5

Smail I., Ivison R. J., Blain A. W., Kneib J.-P., 1998, *ApJ*, **507**, 21

Soifer B. T., Neugebauer G., 1991, *Astron. J.*, **101**, 354

Somerville R. S., Primack J. R., Faber S. M., 2001, *MNRAS*, **320**, 504

Spitzer L., 1958, *ApJ*, **127**, 17

Steidel C. C., Adelberger K. L., Giavalisco M., Dickinson M., Pettini M., 1999, *ApJ*, **519**, 1

Sugiyama N., 1995, *ApJ Suppl.*, **100**, 281

Tan J. C., Silk J., Balland C., 1999, *ApJ*, **522**, 579

Thornton K., Gaudlitz M., Janka H. T., Steinmetz M., 1998, *ApJ*, **500**, 95

Tresse L., Maddox S., 1998, *ApJ*, **495**, 691

Treyer M. A., Ellis R. S., Milliard B., Donas J., Bridges T. J., 1998, *MNRAS*, **300**, 303

Weir N., Djorgovski S., Fayyad U. M., 1995, *Astron. J.*, **110**, 1

White S. D. M., Frenk C. S., 1991, *ApJ*, **379**, 52

Williams R. E., et al., 1996, *Astron. J.*, **112**, 1335